Redox Characteristics of Nickel and Palladium Complexes of the Open-Chain Tetrapyrrole Octaethylbilindione: A Biliverdin Model

Pamela A. Lord, Marilyn M. Olmstead, and Alan L. Balch*

Department of Chemistry, University of California, Davis, California 95616

Received August 24, 1999

Octaethylbiliverdin, $C_{35}H_{46}N_4O_2$, is a linear tetrapyrrole that can exist in coordinated form as the fully reduced trianion $(OEB)^{3-}$, as the two electron oxidized monoanion, $(OEBOx)^-$, or as the one electron oxidized radical, $(OEB^{\bullet})^{2-}$. The three-membered electron-transfer series involving $[M(OEB)]^n$ with n = +1, 0, and −1, and M = Ni or Pd has been characterized electrochemically. The most highly oxidized members of these series have been isolated in the form of their diamagnetic triiodide salts, $[Ni^{II}(OEBOx)]I_3$ and $[Pd^{II}(OEBOx)]I_3$, and characterized spectroscopically and by X-ray diffraction. $[Ni^{II}(OEBOx)]I_3$ crystallizes in the orthorhombic space group *Pbcn* with $a = 15.121(3)$ Å, $b = 16.777(3)$ Å, and $c = 14.628(3)$ Å at 130(2) K with $Z = 4$. Refinement of 3311 reflections with 209 parameters and no restraints yielded wR2 = 0.136 and R = 0.054 for 2643 reflections with $I > 2\sigma(I)$. The structure involves helical coordination of the linear tetrapyrrole ligand about the nickel with all four nitrogen atoms coordinated to the metal and Ni−N distances of 1.867(5) and 1.879(5) Å. The triiodide ion is not coordinated to the nickel but sits over one of the meso carbon atoms of the tetrapyrrole. In the solid state, pairs of $[Ni^{II}(OEBOx)]^+$ crystallize about a center of symmetry so that two identical tab/slot hydrogen-bonded arrangements involving the lactam oxygen of one complex and methine and two methylene protons of the adjacent cation. Similar hydrogen-bonded motifs are found in other complexes derived from octaethylbilindione. $[Pd^{II}(OEBOx)]I_3$ is isomorphic with the nickel analogue and crystallizes in the orthorhombic space group *Pbcn* with $a = 15.2236(6)$ Å, $b = 16.7638(7)$ Å, and $c = 14.6289(6)$ Å at 90(2) K with $Z = 4$. Refinement of 6123 reflections with 209 parameters and no restraints yielded wR2 = 0.094 and R = 0.036 for 4042 reflections with $I > 2\sigma(I)$. The odd electron compound $Pd^{II}(OEB^{\bullet})$ has also been isolated and characterized by single-crystal X-ray diffraction. Black $Pd^{II}(OEB^{\bullet})$ crystallizes in the monoclinic space group *I*2/*a* with $a = 13.274(3)$ Å, $b = 18.655(4)$ Å, $c = 14.114(3)$ Å, and $\beta = 116.00(3)°$ at 140(2) K with Z = 4. Refinement of 2030 reflections with 195 parameters and no restraints yielded wR2 = 0.090 and R = 0.042 for 1715 reflections with $I > 2\sigma(I)$. The structure again involves helical coordination of the linear tetrapyrrole to the palladium through the four pyrrole nitrogen atoms. Reduction of the complex causes a slight elongation of the Pd−N bonds from 1.983(2) and 1.986(2) Å in $[Pd^{II}(OEBOx)]I_3$ to 2.011(4) and 2.012(4) Å in $Pd^{II}(OEB^{\bullet})$.

Introduction

Treatment of $(py)_2Fe(OEP)$ with dioxygen and a reducing agent, hydrazine or ascorbic acid, in pyridine solution results in the oxidative cleavage of the heme ring to form verdoheme and the iron(III) complex of octaethylbilindione, $(py)_2Fe^{III}(OEB)$[1,2] (Chart 1). When the latter complex is isolated by chromatography and removal of pyridine, it is converted into the dimeric complex, $\{Fe^{III}(OEB)\}_2$. The ready loss of iron from $\{Fe^{III}(OEB)\}_2$ has hampered study of the chemistry of this complex. Fortunately complexes of octaethylbilindione (**1**, H_3OEB, Scheme 1) with other metal ions exhibit considerable stability with regard to metal ion dissociation, and the study of these complexes has provided useful information about the nature of the resulting complexes.[3−6]

Chart 1

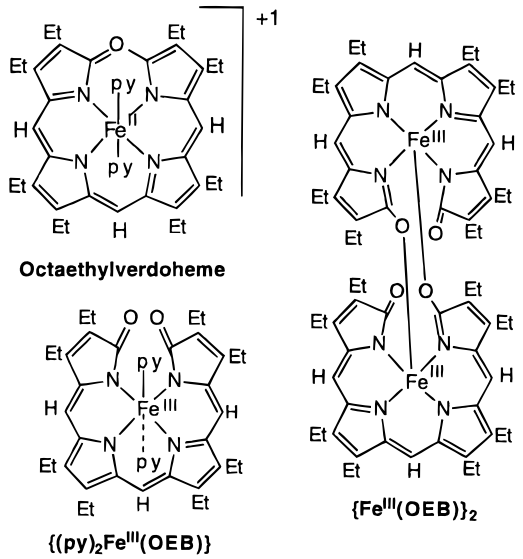

Octaethylbilindione, **1**, is also a convenient model for the bile pigment biliverdin IXα which is formed by heme oxygenase through oxidative attack upon the α-methine position of heme.[7−11] Biliverdin has also been suggested to have both anti-

(1) Balch, A. L.; Latos-Grażyński, L.; Noll, B. C.; Olmstead, M. M.; Safari, N. *J. Am. Chem. Soc.* **1993**, *115*, 9056.
(2) Balch, A. L.; Latos-Grażyński, L.; Noll, B. C.; Olmstead, M. M.; Szterenberg, L.; Safari, N. *J. Am. Chem. Soc.* **1993**, *115*, 1422.
(3) Bonnett, R.; Buckley, D. G.; Hamzetash, D. *J. Chem. Soc., Perkin Trans 1* **1981**, 322.
(4) Balch, A. L.; Mazzanti, M.; Noll, B. C.; Olmstead, M. M. *J. Am. Chem. Soc.* **1994**, *116*, 9114.
(5) Balch, A. L.; Mazzanti, M.; Noll, B. C.; Olmstead, M. M. *J. Am. Chem. Soc.* **1993**, *115*, 12206.
(6) Bonfiglio, J. V.; Bonnett, R.; Buckley, D. G.; Hamzetash, D.; Hursthouse, M. B.; Abdul Malik, K. M.; McDonagh, A. F.; Trotter, J. *Tetrahedron* **1983**, *39*, 1865.

10.1021/ic9910209 CCC: $19.00
Published on Web 03/03/2000

Scheme 1. Redox Behavior of Octaethylbilindione

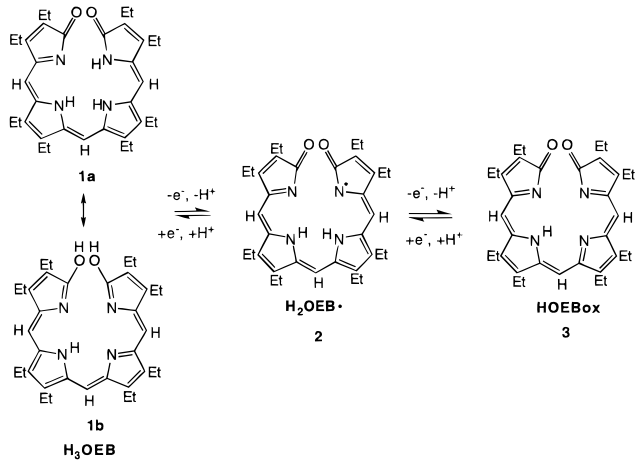

oxidant activity[12] and anti-HIV activity[13,14] and is widely utilized as a pigment by various organisms. Thus, studying the chemical behavior of biliverdin and its synthetic analogues, especially in redox reactions, may lead to a better understanding of these potentially significant physiological roles. Key redox states of this ligand as observed in its complexes are shown in Scheme 1. This laboratory has previously reported that octaethylbilindione undergoes a facile 2-electron oxidation by diiodine to produce an oxidized tetrapyrrole cation, $[H_2OEBOx]^+$.[15] This cation crystallizes as the salt $[H_2OEBOx]I_3 \cdot 0.5\ I_2 \cdot 0.5\ CH_2Cl_2 \cdot 0.2 \cdot C_6H_{14}$, in which two cations are paired through a complex hydrogen bonding network that involves N−H···O hydrogen bonds.

Recently, this laboratory reported that the cobalt complex of octaethylbilindione, whose physical properties suggest that its electronic structure is comprised of resonance components which include Co^{III}(OEB) and Co^{II}(OEB$^\bullet$) electronic distributions, undergoes a series of reversible redox reactions that generate a series of complexes with charges of +1, 0, −1, and −2.[16] The two most oxidized members of this series have been isolated. For the most oxidized species, the complex adopts the electronic structure $[Co^{II}(OEBox)]^+$ in the triiodide salt, $[Co^{II}(OEBox)]I_3$. However the electronic distribution between ligand and metal in this cation is altered by changes in axial ligation.[17] In $[Co^{II}(OEBox)]I_3$ the cobalt ion is four-coordinate, with the triiodide ion relatively far from the cobalt ion. The EPR spectrum of the complex is indicative of the presence of a Co^{II} center within the complex. However, when the salt, $[Co^{II}(OEBox)]I_3$, is dissolved in pyridine solution, there is a marked change in the EPR spectrum of the complex. The electronic structure of the product, which has been isolated and characterized by X-ray crystallography, is best described as $[(py)_2Co^{III}(OEB)]^+$. Here we examine the redox behavior of the nickel and palladium complexes of octaethylbilindione in order to determine the generality of the redox behavior of this group of transition metal complexes. A preliminary report on the novel tetrameric $Pd_4(OEB)_2$, which contains palladium(I) ions π-bonded to C═C bonds of the tetrapyrrole ligand, and of Pd^{II}(OEB$^\bullet$) has appeared.[18] The structure of the nickel complex of octaethylbilindione has also been reported, but at that time the paramagnetic nature of this complex was poorly understood.[6]

Results and Discussion

Chemical and Electrochemical Studies. Ni^{II}(OEB$^\bullet$) was prepared as described previously.[6] The EPR spectrum of the complex shows a resonance at $g = 2.008$. The ^{1}H NMR spectrum revealed only very broad resonances in the 0−3 ppm region, and an assignment was not possible. Pd^{II}(OEB$^\bullet$) was obtained by dissolving $Pd_4(OEB)_2$ in pyridine and allowing ethanol to diffuse into the solution as reported earlier[18] or as reported here directly from H_3OEB by metalation with limited amounts of palladium(II) acetate. As with the nickel analogue, the NMR spectrum of Pd^{II}(OEB$^\bullet$) showed only broad resonances in the 0−3 ppm range, but an EPR spectrum with $g = 2.003$ was observed. The UV/vis absorption spectra of Ni^{II}(OEB$^\bullet$) and Pd^{II}(OEB$^\bullet$) are shown in Figure 1.

Figure 2 shows cyclic voltammetric curves and Osteryoung square-wave voltammetric data for Ni^{II}(OEB$^\bullet$) and Pd^{II}(OEB$^\bullet$) in dichloromethane solution, and Table 1 presents some comparative electrochemical data. Each complex exhibits a reversible (or nearly reversible in the case of the palladium complex) oxidation with experimental values of ΔE_p and $W_{1/2}$ that are close to the theoretical values of 59 and 125 mV which are expected for reversible, one-electron processes. Ni^{II}(OEB$^\bullet$) shows a reversible reduction at −692 mV that is followed by a second reversible reduction at −2095 mV. The clean, reversible nature of the redox processes suggests that major changes in the coordination environment do not occur during the electron-transfer processes. For Pd^{II}(OEB$^\bullet$) only a single reduction is observed at −667 mV. Comparable electrochemical data for the free ligand, octaethylbilindione (H_3OEB), reveal an irreversible oxidation at +200 mV and an irreversible reduction at −1700 mV.[15] Thus both Ni^{II}(OEB$^\bullet$) and Pd^{II}(OEB$^\bullet$) are more easily oxidized and more easily reduced than the free ligand, octaethylbilindione. As noted above the chemical oxidation of octaethylbilindione results in a two-electron oxidation. Comparison of the electrochemical data in Table 1 for the three complexes, Ni^{II}(OEB$^\bullet$), Pd^{II}(OEB$^\bullet$), and Co^{II}(OEB$^\bullet$), shows that the processes seen for the +1/0, 0/−1, and −1/−2 redox processes occur at similar potentials (with the exception of the absence of the −1/−2 process for the palladium complex). These similarities suggest that the electrochemical processes are largely dominated by the redox characteristics of the coordinated ligand.

Chemically, the oxidation of Ni^{II}(OEB$^\bullet$) and Pd^{II}(OEB$^\bullet$) can be accomplished by the addition of diiodine to dichloromethane solutions of the complexes. Addition of diethyl ether to the resulting solutions produces the salts, $[Ni^{II}(OEBOx)]I_3$ and $[Pd^{II}(OEBOx)]I_3$, as black crystalline solids that are slightly more soluble in dichloromethane than in chloroform. Figure 1 shows

(7) O'Carra, P. In *Porphyrins and Metalloporphyrins*; Smith, K. M., Ed.; Elsevier: New York, 1975; p 123.
(8) Schmid, R.; McDonagh, A. F. In *The Porphyrins*; Dolphin, D., Ed.; Academic Press: New York, 1979; Vol. 6, p 257.
(9) Brown, S. B. In *Bilirubin*; Heirwegh, K. P. M., Brown, S. B., Eds.; CRC Press: Boca Raton, FL, 1982; Vol. 2, p 1.
(10) Bissell, D. M. In: *Liver: Normal Function and Disease. Bile Pigments and Jaundice*; Ostrow, J. D., Ed.; Marcel Dekker: New York, 1986; Vol. 4, p 133.
(11) Maines, M. D. *Heme Oxygenase: Clinical Applications and Functions*; CRC Press: Boca Raton, FL, 1992.
(12) Stocker, R.; Yamamoto, Y.; McDonagh, A. F.; Glazer, A. N.; Ames, B. N. *Science* **1987**, *235*, 1043.
(13) Nakagami, T.; Taji, S.; Takahashi, M.; Yamanishi, K. *Microbiol. Immunol.* **1992**, *36*, 381.
(14) Mori, H.; Otake, T.; Morimoto, M.; Ueba, N.; Kunita, N.; Nakagami, T.; Yamasaki, N.; Taji, S. *Jpn. J. Cancer Res.* **1991**, *82*, 755.
(15) Balch, A. L.; Koerner, R.; Olmstead, M. M.; Mazzanti, M.; Safari, N.; St. Claire, T. *J. Chem. Soc., Chem. Commun.* **1995**, 643.
(16) Attar, S.; Balch, A. L.; Van Calcar, P. M.; Winkler, K. *J. Am. Chem. Soc.* **1997**, *119*, 3317.
(17) Attar, S.; Ozarowski, A.; Van Calcar, P. M.; Winkler, K.; Balch, A. L. *Chem. Commun.* **1997**, 1115.
(18) Lord, P.; Olmstead, M. M.; Balch, A. L. *Angew. Chem., Int. Ed.* **1999**, *38*, 2761.

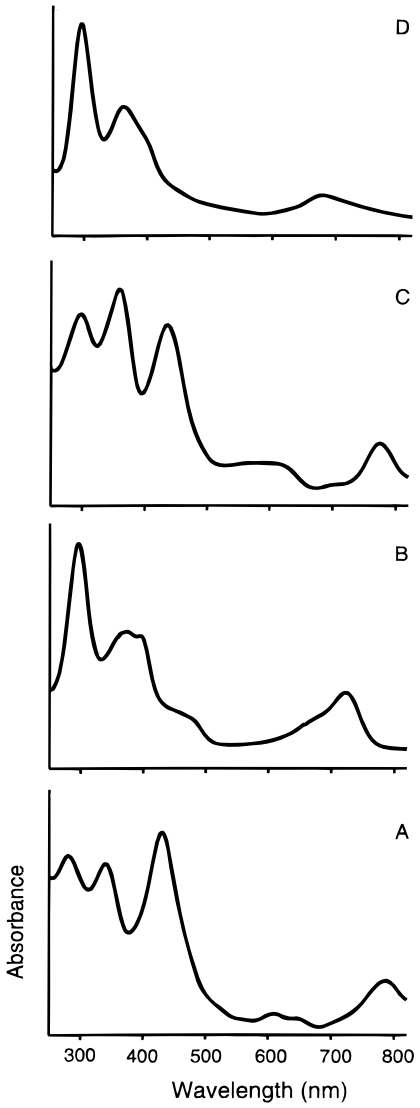

Figure 1. Electronic absorption spectra: A, $Pd^{II}(OEB^{\bullet})$ in chloroform, λ_{max} (nm) (ϵ, M^{-1} cm^{-1}) = 788 (1.09 × 10^4), 646 (4.60 × 10^3), 608 (5.13 × 10^3), 430 (3.33 × 10^4), 342 (2.56 × 10^4), 284 (2.40 × 10^4); B, $[Pd^{II}(OEBox)]I_3$ in dichloromethane, λ_{max} (nm) (ϵ, M^{-1} cm^{-1}) = 724 (1.75 × 10^4), 676 (sh, 1.00 × 10^4), 460 (1.16 × 10^4), 394 (3.263 × 10^4), 374 (3.30 × 10^4), 296 (4.93 × 10^4); C, $Ni^{II}(OEB^{\bullet})$ in chloroform, λ_{max} (nm) (ϵ, M^{-1} cm^{-1}) = 773 (7.7 × 10^3), 600 (plateau 570−620) (7.0 × 10^3), 435 (2.21 × 10^4), 361 (2.56 × 10^4), 300 (2.1 × 10^4); D, $[Ni^{II}(OEBox)]I_3$ in dichloromethane, λ_{max} (nm) (ϵ, M^{-1} cm^{-1}) = 742 (sh, 3.17 × 10^3), 678 (5.90 × 10^3), 446 (sh, 6.52 × 10^3), 402 (sh, 1.72 × 10^4), 362 (2.48 × 10^4), 296 (3.91 × 10^4).

the UV/vis absorption spectra of $[Ni^{II}(OEBOx)]I_3$ and $[Pd^{II}(OEBOx)]I_3$ in dichloromethane solutions. The ^1H NMR spectra of $[Ni^{II}(OEBOx)]I_3$ show resonances that are characteristic of a diamagnetic complex with meso resonances as singlets at 7.53 and 7.26 ppm, complex methylene resonances in the range 3.00−2.42 ppm, and methyl resonances in the range 1.43−1.12 ppm. $[Pd^{II}(OEBOx)]I_3$ shows a similar ^1H NMR spectrum: meso resonances at 7.50 and 7.29 ppm, complex methylene resonances in the range 2.98−2.49 ppm, and methyl resonances in the range 1.18−1.43 ppm.

The UV/vis absorption spectra of $[Ni^{II}(OEBOx)]I_3$ or $[Pd^{II}(OEBOx)]I_3$ in pyridine solution undergo a gradual changes which indicate that reduction occurs to form $[Ni^{II}(OEB^{\bullet})]$ or $[Pd^{II}(OEB^{\bullet})]$, respectively. Consequently, it appears that pyridine induces the reduction of these complex cations rather than binding to the metal ions and effecting the electronic distribution between the ligand and metal as it does with $[Co^{II}(OEBOx)]I_3$, where $[(py)_2Co^{II}(OEBOx)]I_3$ is formed.[17]

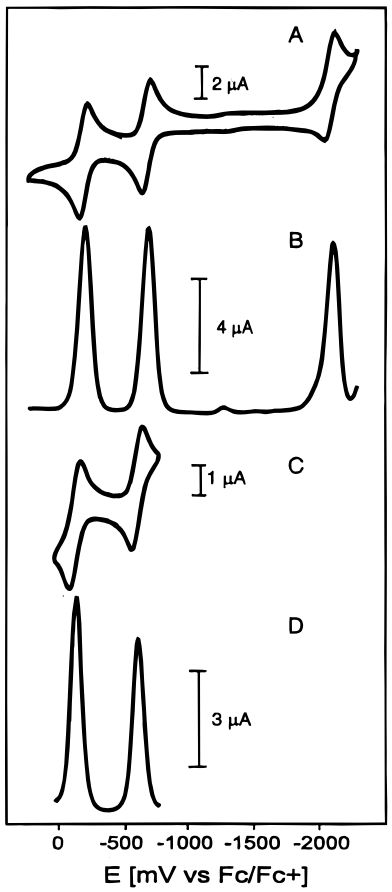

Figure 2. Cyclic voltammograms and Osteryoung square wave voltammograms for (A, B) $Ni^{II}(OEB^{\bullet})$ and C, D) $Pd^{II}(OEB^{\bullet})$ in dichloromethane solution with 0.10 M tetra-*n*-butylammonium perchlorate as supporting electrolyte and referenced to the ferrocene/ferrocinium couple.

Table 1. Electrochemical Data

	oxidn			1st redn			2nd redn		
	E^a	ΔE_p	$W_{1/2}$	E^a	ΔE_p	$W_{1/2}$	E^a	ΔE_p	$W_{1/2}$
$Ni^{II}(OEB^{\bullet})$	−209.5	57	113.5	−692	62	113.4	−2095	57	113.4
$Pd^{II}(OEB^{\bullet})$	−167	94	99.2	−667	73	94.1	not observed		
$Co^{II}(OEB^{\bullet})^b$	−152	59	123	−784	60	122	−2076	65	126

[a] Average E_p(ox) and E_p(red). [b] Data taken from: Attar, S.; Balch, A. L.; Van Calcar, P. M.; Winkler, K. *J. Am. Chem. Soc.* **1997**, *119*, 3317.

Molecular Structure of $[Pd^{II}(OEB^{\bullet})]$. The structure of this complex has been determined by X-ray crystallography. A perspective view of the molecule is shown in Figure 3. Selected interatomic distances and angles are given in Table 2.

The molecule resides on a 2-fold rotation axis which passes through the palladium atom and the meso carbon atom, C(10). The palladium atom is coordinated by the four nitrogen atoms of the tetrapyrrole ligand. The two crystallographically distinct Pd−N distances, 2.011(4) and 2.012(4) Å, have identical lengths within experimental error. The PdN_4 unit shows the following deviations from planarity: Pd, 0.00; N(1), +0.22; N(2), −0.23 Å. The distortion of the palladium coordination from planarity is also seen in the nonlinearity of the trans N(1)−Pd−N(2′) angle, 167.03(16)°, and is a consequence of the restraints placed on the complex by the ligand. The ligand cannot assume a planar geometry because of the overlap of the lactam oxygen atoms,

Table 2. Selected Bond Distances and Angles

	$Ni^{II}(OEB^{\bullet})^a$	$[Ni^{II}(OEBox)]I_3$	$Pd^{II}(OEB^{\bullet})$	$[Pd^{II}(OEBox)]I_3$
		Bond Distances (Å)		
M−N(1)	1.875(7)	1.867(5)	2.012(4)	1.983(2)
M−N(2)	1.897(7)	1.879(5)	2.011(4)	1.986(2)
C(1)−O(1)	1.248(9)	1.198(7)	1.223(6)	1.204(3)
I(1)−I(2)		2.9338(8)		2.9343(4)
		Bond Angles (deg)		
N(1)−M−N(2)		90.0(2)	89.42(15)	88.61(10)
N(1)−M−N(1′)	92.9(3)	92.7(3)	93.5(2)	93.79(14)
N(2)−M−N(2′)		92.7(3)	90.6(2)	91.59(14)
N(1)−M−N(2′)	162.1(3)	162.3(2)	167.03(16)	167.72(10)
I(2)−I(1)−I(2′)		178.95(3)		179.464(17)

[a] Data from: Bonfiglio, J. V.; Bonnett, R.; Buckley, D. G.; Hamzetash, D.; Hursthouse, M. B.; Abdul Malik, K. M.; McDonagh, A. F.; Trotter, J. *Tetrahedron* **1983**, *39*, 1865.

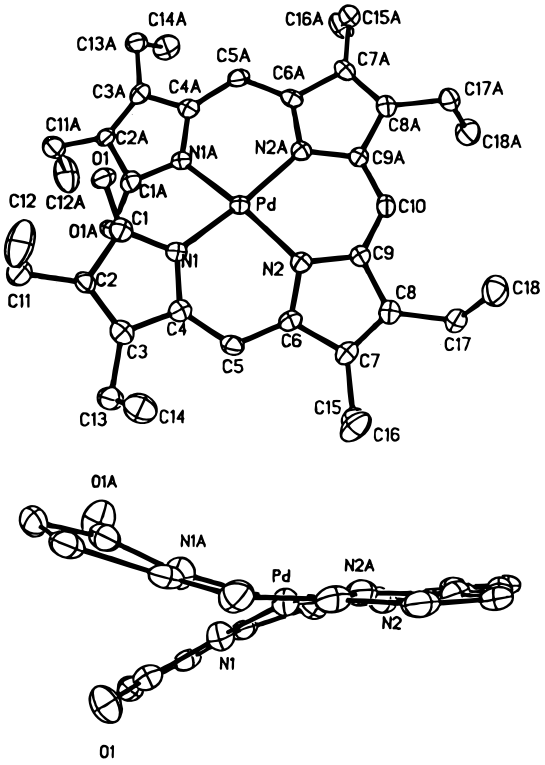

Figure 3. Top: Perspective view of $Pd^{II}(OEB^{\bullet})$ with 50% thermal contours for all non-hydrogen atoms. Bottom: View looking edge-on at the planar portion that consists of the pyrrole rings which contain N(2) and N(2A). For clarity the ethyl groups were omitted.

and as a result, it assumes a helical structure. Related helical structures are found in other complexes obtained from octaethylbilindione. The C(1)−O(1) bond distance, 1.223(6) Å, is consistent with the presence of a C═O group at the end of the ligand.

Molecular Structures of $[Ni^{II}(OEBox)]I_3$ and $[Pd^{II}(OEBox)]I_3$. Crystals of $[Ni^{II}(OEBox)]I_3$ and $[Pd^{II}(OEBox)]I_3$ are isomorphic. The structures of both have been determined by X-ray crystallography, and that for $[Ni^{II}(OEBox)]I_3$ is shown in Figure 4. Selected interatomic distances and angles for both $[Ni^{II}(OEBox)]I_3$ and $[Pd^{II}(OEBox)]I_3$ are given in Table 2 where they can be compared to those of $Ni^{II}(OEB^{\bullet})$ and $Pd^{II}(OEB^{\bullet})$.

The cation resides on a 2-fold rotation axis which passes through the nickel atom and the meso carbon atom, C(10). The nickel atom is coordinated to each of the four nitrogen atoms of the ligand. The two crystallographically distinct Ni−N distances are 1.867(5) and 1.879(5) Å and are only marginally shorter than the corresponding distances in $Ni^{II}(OEB^{\bullet})$. The NiN_4 unit is distorted from planarity by the ligand constraints with

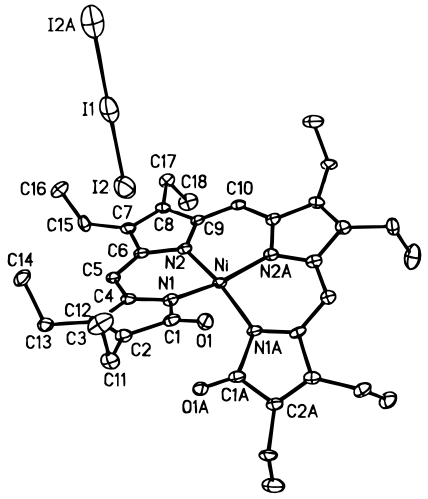

Figure 4. Perspective view of $[Ni^{II}(OEBox)]I_3$ with 50% thermal contours for all non-hydrogen atoms.

the following deviations from the molecular plane: Ni, 0.00; N(1), −0.29; N(2), +0.29 Å. The trans N(1)−Ni−N(2′) angle is 162.3(2)°.

The triiodide ion is not coordinated to the nickel ion. The shortest Ni−I distance is 4.865 Å. The triiodide ligand sits with the central iodine atom, I(1), on a crystallographic 2-fold axis. The I−I distance (2.9338(8) Å) is normal, and the triiodide ion is nearly linear with an I(2)−I(1)−I(2′) angle of 178.95(3)°.

As seen in Table 2, the geometry of the cation in $[Pd^{II}(OEBox)]I_3$ is similar to that of the isomorphic nickel analogue and the triiodide ion is not coordinated. The shortest Pd···I distance is 4.965 Å. Again the palladium ion does not have completely planar geometry, but the distortions are somewhat less than those seen for the nickel corresponding complex. The deviations from planarity within the PdN_4 unit are only 0.00 Å for Pd, −0.21 Å for N(1), and +0.21 Å for N(2). The N(1)−Pd−N(2′) angle, 167.72(10)°, is somewhat wider than the corresponding angle, 162.3(2)°, in $[Ni^{II}(OEBox)]I_3$.

The C(1)−O(1) bond distances, 1.198(7) and 1.204(3) Å for the nickel- and palladium containing cations, $[Ni^{II}(OEBox)]I_3$ and $[Pd^{II}(OEBox)]I_3$, are consistent with the presence of a C═O groups at the end of the ligand in each complex.

Solid-State Packing in $Pd^{II}(OEB^{\bullet})$, $[Ni^{II}(OEBox)]I_3$, and $[Pd^{II}(OEBox)]I_3$. A common supramolecular structural element, which involves a tab/slot interaction between the lactam oxygen of one molecule with a pocket of three C−H hydrogen bond donors, has been found to dominate the solid-state structures of a number of complexes obtained from octaethylbilindione.[16] The C−H hydrogen bond donors consist of a meso C−H group

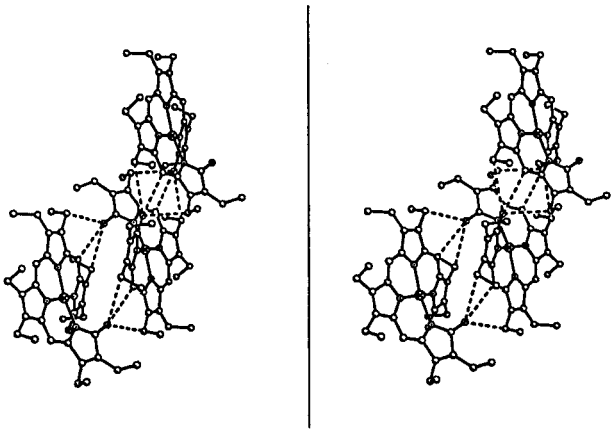

Figure 5. Stereoview of three molecules of $Pd^{II}(OEB^{\bullet})$ which shows the twisted chain produced by tab/slot interactions between the molecules.

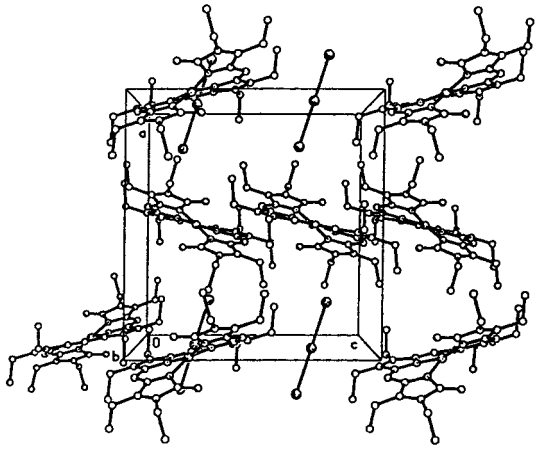

Figure 6. View of the unit cell of $[Ni^{II}(OEBox)]I_3$ which shows positioning of the triiodide ions and the tab/slot interactions between the cations.

and two methylene C−H groups from the adjacent ethyl groups. This tab/slot feature is also present in the structure of $Pd^{II}(OEB^{\bullet})$, where each oxygen atom is involved in a tab/slot hydrogen bonding arrangement. Figure 5 shows the interactions between three molecules of $Pd^{II}(OEB^{\bullet})$. These interactions lead to the organization of individual $Pd^{II}(OEB^{\bullet})$ molecules into chains, but the twisted chains in this structure differ from the linear chains observed earlier for $M^{II}(OEB^{\bullet})$, M = Ni, Co, and Cu.[16]

The tab/slot arrangement is also found to be a significant part of the solid-state organization in $[Ni^{II}(OEBox)]I_3$ and in $[Pd^{II}(OEBox)]I_3$. Figure 6 shows the contents of the unit cell for $[Ni^{II}(OEBox)]I_3$. As the drawing shows, each cation participates in two tab/slot interactions with neighboring cations to form linear arrays of cations. Similar chains have been seen previously in the solid-state structure of the neutral complexes, $M^{II}(OEB^{\bullet})$ with M = Co, Ni, and Cu. Within these chains the O···C(meso) and O···C(methylene) distances are 3.516, 3.695, and 3.642 Å for $[Ni^{II}(OEBox)]I_3$ and 3.648, 3.536, and 3.803 Å for $[Pd^{II}(OEBox)]I_3$. The C···O distances involved in these arrangements are ca. 3.6 Å; thus, they are consistent with previously determined cases of C−H···O hydrogen bonds.[19,20,21]

As seen in Figures 4 and 6, it is clear that the triiodide ions are well separated from the complex cations in $[Ni^{II}(OEBox)]I_3$ and $[Pd^{II}(OEBox)]I_3$. The closest approach of the triiodide ion to the $[Ni^{II}(OEBox)]^+$ involves contact with a C=C bond that is exocyclic to the pyrrole ring that contains N(1). Thus I(2) is positioned 3.890 Å from C(4) and 4.274 Å from C(5). Similarly in $[Pd^{II}(OEBox)]I_3$, I(2) is positioned 3.966 Å from C(4) and 4.318 Å from C(5). A related orientation of a triiodide ion and a porphyrin cation has been seen in the salt $[H_3OEP]I_3 \cdot C_6H_6$.[22] In that case, the triiodide ion also is situated nearly perpendicular to the porphyrin plane and makes contact at a C=C bond which is again exocyclic to a pyrrole ring. The I···C distances in this case are 3.770 and 4.063 Å. The orientation of the triiodide ion and the metal-containing cation in $[Pd^{II}(OEBox)]I_3$ is markedly different from that seen in the related salt, $[Co^{II}(OEBox)]I_3$. In the latter salt, one end of the triiodide ion is much closer to the cobalt ion with Co···I distances of 2.818(4), 2.875(10), and 2.798(14) Å for the three disordered triiodide sites.

Discussion

This work demonstrates that the redox properties first observed for the cobalt complexes obtained from octaethylbilindione are found with other metal ions as well and appear to be a general property of this ligand system. For nickel, the four-membered redox series involving complexes with charges of +1, 0, −1, and −2 has been established and the two most oxidized complexes, which have been isolated, have electronic structures that are well represented as $[Ni^{II}(OEBox)]^+$ and $Ni^{II}(OEB^{\bullet})$. For palladium, a three-membered redox series involving complexes with charges of +1, 0, and −1 has been observed, and the two most oxidized members have electronic structures represented by the formulas $[Pd^{II}(OEBox)]^+$ and $Pd^{II}(OEB^{\bullet})$.

The redox behavior of these complexes obtained from octaethylbilindione is related to that of a number of other ligands. The simplest analogues are the dioxolene complexes derived from the quinone/catecholate redox system (Chart 2).

Chart 2

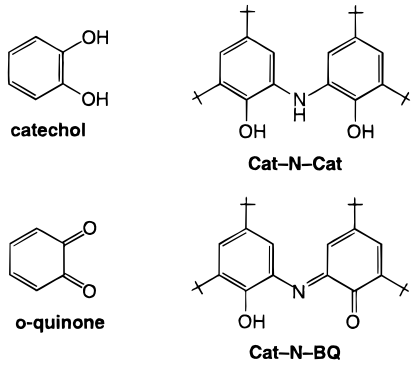

The redox behavior of dioxolene complexes has been extensively documented,[23−27] as has the redox behavior of their nitrogen counterparts.[28] A number of tautomeric structures can be drawn for octaethylbiliverdin and its oxidation product, HOEBox. The structures **1a** and **3** shown in Scheme 1 were drawn to emphasize the relationship of the H_3OEB/HOEB and

(19) Taylor, R.; Kennard, O. *J. Am. Chem. Soc.* **1982**, *104*, 5063.
(20) Sarma, J. A. R. P.; Desiraju, G. R. *Acc. Chem. Res.* **1986**, *19*, 222.
(21) Desiraju, G. R. *Acc. Chem. Res.* **1991**, *24*, 290.
(22) Hirayama, N.; Takenaka, A.; Sasada, Y.; Watanabe, E.-I.; Ogoshi, H.; Yoshida, Z.-I. *Bull. Chem. Soc. Jpn.* **1981**, *54*, 998.
(23) Rohrscheid, F.; Balch, A. L.; Holm, R. H. *Inorg. Chem.* **1966**, *5*, 1542.
(24) Sohn, Y. S.; Balch, A. L. *J. Am. Chem. Soc.* **1972**, *94*, 1144.
(25) Pierpont, C. G.; Lange, C. W. *Prog. Inorg. Chem.* **1994**, *41*, 331.
(26) Jung, O.-S.; Jo, D. H.; Lee, Y.-A.; Sohn, Y. S.; Pierpont, C. G. *Inorg. Chem.* **1998**, *37*, 5875.
(27) Lange, C. W.; Pierpont, C. G. *Inorg. Chim. Acta* **1997**, *263*, 219.
(28) Balch, A. L.; Holm, R. H. *J. Am. Chem. Soc.* **1966**, *88*, 5201.

Table 3. Crystallographic Data

	$Pd^{II}(OEB^{\bullet})$	$[Ni^{II}(OEBox)]I_3$	$[Pd^{II}(OEBox)]I_3$
formula	$C_{35}H_{43}N_4O_2Pd$	$C_{35}H_{43}I_3N_4NiO_2$	$C_{35}H_{43}I_3N_4PdO_2$
fw	658.13	991.14	1038.83
a, Å	13.274(3)	15.121(3)	15.2236(6)
b, Å	18.655(4)	16.777(3)	16.7638(7)
c, Å	14.113(3)	14.628(3)	14.6289(6)
α, deg	90	90	90
β, deg	116.00(3)	90	90
γ, deg	90	90	90
V, Å^3	3141.3(11)	3710.9(13)	3733.4(3)
Z	4	4	4
cryst system	monoclinic	orthorhombic	orthorhombic
space group	*I*2/*a*	*Pbcn*	*Pbcn*
T, K	140(2)	130(2)	90(2)
λ, Å	0.710 73 (Mo Kα)	1.541 78 (Cu Kα)	0.710 73 (Mo Kα)
ρ, g/cm^3	1.392	1.774	1.848
μ, mm^{-1}	0.628	20.624	3.013
max and min transm	0.95−0.77	0.289−0.054	0.876−0.486
R1 (obsd data)[a]	0.042	0.054	0.036
wR2 (all data, F^2 refinement)[b]	0.090	0.136	0.094

[a] $R1 = \sum||F_o| - |F_c||/\sum|F_o|$, observed data ($>4\sigma(I_o)$). [b] $wR2 = [\sum[\omega(F_o^2 - F_c^2)^2]/\sum[\omega(F_o^2)^2]]^{1/2}$, all data.

the catechol/quinone redox systems. Similarily, the Cat-N-Cat/Cat-N-BQ redox couple also shown in Chart 2 produces several interesting series of transition metal complexes that can exist in a multiplicity of redox states due to largely ligand based processes.[29−31]

In the solid state, complexes derived from H_3OEB or $[H_2OEBOx]^+$ form supramolecular arrays through C−H···O hydrogen bonds that involve association through the tab/slot scheme shown in Figures 5 and 6. This packing arrangement can result in the formation of discrete pairs of molecules (or ions) that form about a center of symmetry with only one lactam oxygen of each ligand participating in hydrogen bonding. Alternatively, a linear chain of complexes can form in which both lactam oxygen atoms function as hydrogen bond acceptors. Interestingly, $[Co^{II}(OEBox)]I_3$ crystallizes so that the complex cations associate pairwise while $[Ni^{II}(OEBox)]I_3$ and $[Pd^{II}(OEBox)]I_3$ crystallize to form linear chains with both lactam oxygen atoms involved in the tab/slot hydrogen bonding motif. Since centrosymmetric arrangements are involved in both cases, the pairs of complexes or the linear chains contain equal numbers of helical complexes with opposite senses chirality. Thus, crystallization produces a racemic mixture within each solid. For $Pd^{II}(OEB^{\bullet})$, $[Ni^{II}(OEBox)]I_3$, and $[Pd^{II}(OEBox)]I_3$ the crystals are centrosymmetric, and hence, each crystal contains a racemate of the helical complexes.

Experimental Section

Preparation of Compounds. $Ni^{II}(OEB^{\bullet})$ was prepared as previously reported.[6]

H_3OEB. Samples of $ClFe^{III}(OEP)$ (200 mg, 0.32 mmol) and ascorbic acid (750 mg, 4.3 mmol) were dissolved in a mixture of 50 mL of dichloromethane and 50 mL of pyridine. This red solution was stirred for 2 min. Dioxygen was then vigorously bubbled through the solution until it turned green. The solution was filtered and the solvent removed. The resulting residue was dissolved in methanol (25 mL). A 10 mL portion of a 10% KOH in methanol solution was added, and the solution was stirred for 2 min. A 30 mL portion of a 25% HCl solution in methanol was added, and the mixture was heated under reflux for 10 min. The blue solution was filtered and concentrated to 10 mL. The concentrated solution was dissolved in chloroform (50 mL), washed with water (3 × 100 mL), dried over Na_2SO_4, filtered, and evaporated to dryness. The resulting solid was dissolved in chloroform, and filtered through a 5-cm thick layer of Celite and alumina, and concentrated. This chloroform solution was subjected to chromatography on a silica column. The product, H_3OEB, was eluted as a dark blue band with chloroform as the eluent. The product was recrystallized using chloroform and petroleum ether: yield 63 mg, 35%.

$[Ni^{II}(OEBox)]I_3$. A solution of diiodine (27.7 mg, 0.110 mmol) in 10 mL of dichloromethane was added dropwise to a solution of $Ni^{II}(OEB^{\bullet})$ (33.1 mg, 0.054 mmol) in 10 mL of dichloromethane, and the mixture was stirred for 30 min. The solvent was removed. The resulting residue was dissolved in a minimal volume of dichloromethane and layered with pentane. Upon standing overnight, the solution was filtered and black crystals were collected, washed with pentane, and vacuum-dried: yield 44.5 mg, 82.8%. Crystals suitable for crystallography were grown by slow diffusion of diethyl ether into a dichloromethane solution of the complex.

$Pd^{II}(OEB^{\bullet})$. Under a dinitrogen atmosphere, a solution of palladium(II) acetate (28.2 mg, 0.126 mmol) in 5 mL of chloroform was added to a solution of octaethylbiliverdin (28.8 mg, 0.052 mmol) in 25 mL of ethanol. After being heated to 65 °C for 5 min followed by stirring for 30 min, the solvent was evaporated. The resulting residue was dissolved in chloroform (50 mL), washed with water (3 × 100 mL), dried over Na_2SO_4, filtered, and evaporated to dryness. The green solid was subject to chromatography on silica (2.5 × 14 cm) with 1% ethanol in chloroform as the eluent. The first dark green band contained $Pd_4(OEB)_2$: yield 16.1 mg, 40.6%. The second dark green band was collected and evaporated to dryness to give $Pd^{II}(OEB^{\bullet})$: yield 16.9 mg, 49.8%.

$[Pd^{II}(OEBox)]I_3$. $[Pd(OEB)]I_3$ was prepared by the procedure used for $[Ni(OEB)]I_3$, yield 83.2%. Crystals suitable for crystallography were grown by slow diffusion of diethyl ether into a dichloromethane solution of the complex.

Instrumentation. ^1H NMR spectra were recorded on a General Electric QE-300 FT spectrometer operating in the quadrature mode (^1H frequency is 300 MHz). The residual ^1H spectrum of chloroform-*d* or dichloromethane-d_2 was used as a secondary reference. Electronic spectra were obtained using a Hewlett-Packard diode array spectrometer.

Cyclic Voltammetry: Dc-cyclic and Osteryoung square-wave voltammetry were performed using the BAS CV-50W potentiostat in a three-electrode cell. The working electrode was a gold wire (Bioanalytical system) with a diameter of 1.5 mm. Before each experiment the electrode was polished with fine carborundum paper and 0.5 μm alumina slurry in sequence. The electrode was then sonicated in order to remove the traces of alumina from the surface, washed with water, and dried. A silver wire immersed in 0.01 M $AgNO_3$ and 0.09 M tetra-*n*-butylammonium perchlorate (TBAP) in acetonitrile and separated

(29) Girgis, A. Y.; Balch, A. L. *Inorg. Chem.* **1975**, *14*, 2724.
(30) Larsen, S. K.; Pierpont, C. G. *J. Am. Chem. Soc.* **1988**, *110*, 1827.
(31) Chaudhuri, P.; Hess, M.; Hildenbrand, K.; Bill, E.; Weyhermüller, T.; Wieghardt, K. *Inorg. Chem.* **1999**, *38*, 2781.

from the working solution by a ceramic tip (Bioanalytical Systems) served as the reference electrode. Potentials are expressed by reference to the ferrocene/ferrocenium redox system. The counter electrode was a platinum wire with an area of ~0.1 cm^2. Tetra-*n*-butylammonium perchlorate (0.10 M) served as the supporting electrode.

X-ray Data Collection. The crystals were removed from the glass tubes together with a small amount of mother liquor and immediately coated with a hydrocarbon oil on the microscope slide. Suitable crystals were mounted on glass fibers with silicone grease and for Pd(OEB) placed in the cold stream of a Siemens R3m/V diffractometer equipped with an Enraf-Nonius low-temperature apparatus. The diffractometer utilized a sealed Mo tube that operated at 2 kW and a graphite monochromator. For $[Ni^{II}(OEB^{\bullet})]I_3$ the crystal was mounted in the 130 K dinitrogen stream of a Syntex $P2_1$ diffractometer equipped with a locally modified low-temperature apparatus. Intensity data were collected using graphite-monochromated Cu Kα radiation (λ, 1.541 78 Å). For $[Pd^{II}(OEB^{\bullet})]I_3$ data were collected on a Bruker SMART CCD with graphite-monochromated Mo Kα radiation at 90(2) K. Lorentz and polarization corrections were applied. Check reflections were stable throughout data collection. Crystal data are given in Table 3.

The structures were solved by direct methods and refined using all data (based on F^2) using the software of SHELXTL, V. 5. For Pd^{II}(OEB) and $[Ni^{II}(OEBox)]I_3$ absorption corrections were applied with the program XABS2 which calculates 24 coefficients from a least-squares fit of ($1/A$ vs $\sin^2(q)$) to a cubic equation in $\sin^2(q)$ by minimization of F_o^2 and F_c^2 differences.[32] For $[Pd^{II}(OEBox)]I_3$ a semiempirical method utilizing equivalents was employed to correct for absorption.[33] Hydrogen atoms were added geometrically and refined with a riding model. All non-hydrogen atoms were refined with anisotropic thermal parameters.

Acknowledgment. We thank the National Institutes of Health (Grant GM26226) for support and Dr. A. Ozarowski, Dr. K. Winkler, and S. Hino for advice and experimental assistance.

Supporting Information Available: Tables of X-ray data and X-ray crystallographic files in CIF format for $Pd^{II}(OEB^{\bullet})$, $[Ni^{II}(OEBox)]I_3$, and $[Pd^{II}(OEBox)]I_3$. This material is available free of charge via the Internet at http://pubs.acs.org.

IC9910209

(32) Parkin, S.; Moezzi, B.; Hope, H. XABS2: An empirical absorption correction program. *J. Appl. Crystallogr.* **1995**, *28*, 53.
(33) Blessing, R. H. *Acta Crystallogr., Sect. A* **1995**, *A51*, 33.